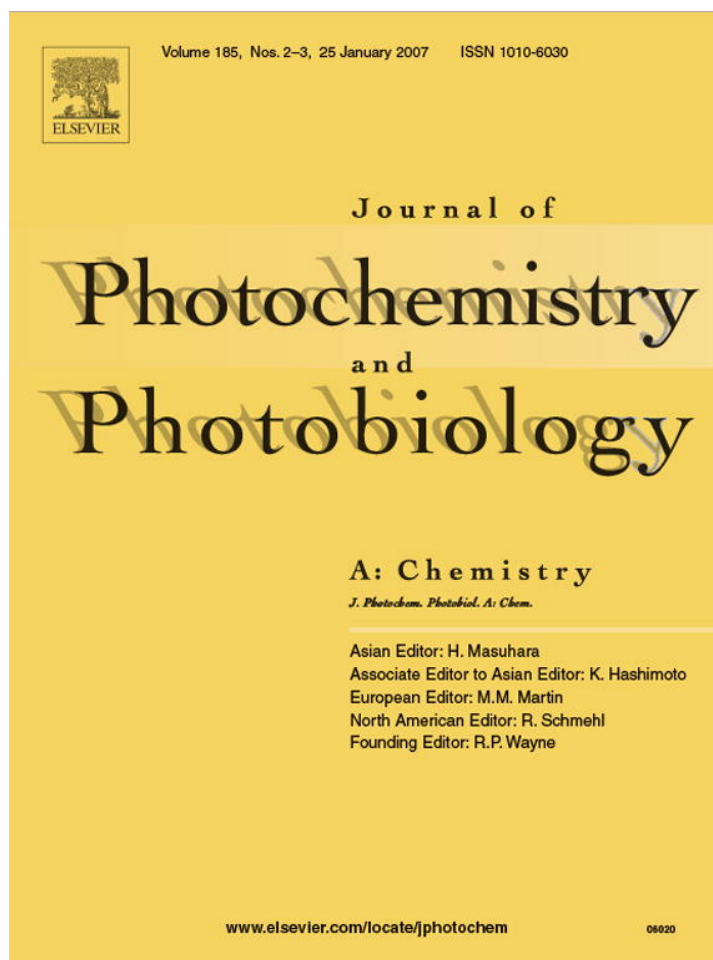


Provided for non-commercial research and educational use only.
Not for reproduction or distribution or commercial use.



This article was originally published in a journal published by Elsevier, and the attached copy is provided by Elsevier for the author's benefit and for the benefit of the author's institution, for non-commercial research and educational use including without limitation use in instruction at your institution, sending it to specific colleagues that you know, and providing a copy to your institution's administrator.

All other uses, reproduction and distribution, including without limitation commercial reprints, selling or licensing copies or access, or posting on open internet sites, your personal or institution's website or repository, are prohibited. For exceptions, permission may be sought for such use through Elsevier's permissions site at:

<http://www.elsevier.com/locate/permissionusematerial>



A mechanism for the photochemical transformation of nitrate in snow

Hans-Werner Jacobi*, Birgit Hilker

Alfred Wegener Institute for Polar and Marine Research, Am Handelshafen 12, 27570 Bremerhaven, Germany

Received 1 June 2006; received in revised form 29 June 2006; accepted 30 June 2006

Available online 8 July 2006

Abstract

Photochemical reactions of trace compounds in snow have important implications for the composition of the atmospheric boundary layer in snow-covered regions and for the interpretation of concentration profiles in snow and ice regarding the composition of the past atmosphere. One of the prominent reactions is the photolysis of nitrate, which leads to the formation of OH radicals in the snow and to the release of reactive nitrogen compounds, like nitrogen oxides (NO and NO₂) and nitrous acid (HONO) to the atmosphere. We performed photolysis experiments using artificial snow, containing variable initial concentrations of nitrate and nitrite, to investigate the reaction mechanism responsible for the formation of the reactive nitrogen compounds. Increasing the initial nitrite concentrations resulted in the formation of significant amounts of nitrate in the snow. A possible precursor of nitrate is NO₂, which can be transformed into nitrate either by the attack of a hydroxy radical or the hydrolysis of the dimer (N₂O₄). A mechanism for the transformation of the nitrogen-containing compounds in snow was developed, assuming that all reactions took place in a quasi-liquid layer (QLL) at the surface of the ice crystals. The unknown photolysis rates of nitrate and nitrite and the rates of NO and NO₂ transfer from the snow to the gas phase, respectively, were adjusted to give an optimum fit of the calculated time series of nitrate, nitrite, and gas phase NO_x with respect to the experimental data. Best agreement was obtained with a ~25 times faster photolysis rate of nitrite compared to nitrate. The formation of NO₂ is probably the dominant channel for the nitrate photolysis. We used the reaction mechanism further to investigate the release of NO_x and HONO under natural conditions. We found that NO_x emissions are by far dominated by the release of NO₂. The release of HONO to the gas phase depends on the pH of the snow and the HONO transfer rate to the gas phase. However, due to the small amounts of nitrite produced under natural conditions, the formation of HONO in the QLL is probably negligible. We suggest that observed emissions of HONO from the surface snow are dominated by the heterogeneous formation of HONO in the firm air. The reaction of NO₂ on the surfaces of the ice crystals is the most likely HONO source to the gas phase.

© 2006 Elsevier B.V. All rights reserved.

Keywords: Photochemical reactions; Snow; Nitrate; Nitrite; Nitrogen oxides

1. Introduction

Photochemical reactions leading to the chemical transformation of trace compounds in the atmosphere do not only occur in the atmospheric gas and liquid phases, but also in the tropospheric ice phase. Such reactions can take place in the upper layers of the natural snow-covers in polar and alpine regions [1]. The photolysis of nitrate (NO₃⁻) was first identified as an important photochemical reaction in this environment [2]. This reaction is considered as one of the key reactions in surface-snow and has been the subject of a series of field [2–17] and laboratory studies [18–27]. Nitrate photoly-

sis has an impact on the composition of and processes in the surface-snow. It also affects the atmosphere after the release of volatile and reactive nitrogen compounds to the gas phase [28,29].

Nitrate is one of the dominating anions found in snow samples in both polar regions [30]. However, the photochemical processing can alter the concentrations in the snow after deposition. Significant losses of nitrate from the surface snow at polar sites with very low snow accumulation rates were attributed to the NO₃⁻ photolysis [24,31]. This effect influences the interpretation of NO₃⁻ profiles in firn and ice cores, which can convolute information obtained about levels of reactive nitrogen compounds in the atmosphere in the past [32]. In addition, NO₃⁻ photolysis can affect further trace compounds in the snow. Laboratory experiments have shown that it leads to the formation of highly reactive hydroxyl (OH) radicals in the snow

* Corresponding author. Tel.: +49 471 4831 1493; fax: +49 471 4831 1425.
E-mail address: hwjacobi@awi-bremerhaven.de (H.-W. Jacobi).

[22] in agreement with well-known aqueous phase processes [33]. The generated OH has the potential to attack organic compounds, eventually leading to the formation of oxidized hydrocarbons like formaldehyde, acetaldehyde, and acetone [1,34,35].

Evidence of the formation of more volatile compounds, which are quickly released to the gas phase, is supported by several field and laboratory studies. Emissions of nitrogen oxides ($\text{NO}_x = \text{NO} + \text{NO}_2$) from the surface snow under the influence of solar radiation have been reported from several Arctic [2,4,11,12], Antarctic [5–7,15], as well as a mid-latitude sites [3]. Nitrous acid (HONO) has also been found to be released from the surface snow at non-marine polar sites [8,11,16], although HONO fluxes from alkaline snow seem to be negligible or even directed to the snow [17,36]. These emissions are driven by the strongly enhanced concentrations of the reactive nitrogen compounds in the interstitial air of the surface snow compared to ambient concentrations [9,14,16]. They have a strong effect on photochemical processes occurring in the atmospheric boundary layer above snow-covered regions. NO_x mixing ratios affected by emissions from the snowpack can reach values on the order of several hundreds of pptV (parts per trillion by volume) under stable atmospheric conditions, even in remote polar regions [7,11,15]. In addition, HONO concentrations up to 70 pptV have been reported for polar regions [8,9,16,17,37]. However, the applied collecting techniques using mist chambers or aqueous scrubbers are prone to interferences for example by pernitric acid (HO_2NO_2), raising concerns about the actual HONO concentrations in polar regions [16,28,38]. Recently, Liao [38] reported simultaneous HONO measurements at South Pole station using laser-induced fluorescence (LIF) and mist chamber-ion chromatography (MC-IC) techniques. They found that the results from the MC-IC measurements were about seven times higher than the LIF measurements. Nevertheless, the reported NO_x and HONO levels have a profound effect on the photochemistry of the polar boundary layer since both compounds are involved in the formation and destruction of OH and hydroperoxyl radicals (HO_2) and ozone [28,29], thus influencing the oxidation capacity of the boundary layer.

Although the strong impact of the NO_3^- photolysis is evident, a full mechanistic understanding of the transformation of nitrogen-containing compounds in the snow is still not available. Previous laboratory studies have focused on different aspects, like the photolytic decomposition of NO_3^- [24,27], the formation of products like OH [20,22] and nitrite (NO_2^-) [19,20,27] and the release of NO_x to the gas phase [18,19,21,23,25,26].

Here, we present a series of laboratory experiments performed with artificial snow samples. Results of photolysis experiments with different initial concentrations of NO_3^- and NO_2^- are used to develop a reaction mechanism for the photochemical transformation of NO_3^- and NO_2^- . The mechanism is further adapted to conditions during previous field experiments performed at Summit, Greenland. The modeled results regarding the emissions of NO_x and HONO are compared to the field measurements, indicating that the main photochemical processes occurring in the natural snow-cover can successfully be reproduced using the proposed mechanism.

2. Experimental methods

Details of the preparation of artificial snow samples have been described previously [27,39]. In short, liquid solutions were prepared from Milli-Q water (resistance larger than $18 \text{ M}\Omega$) by adding sodium nitrate or sodium nitrite (both Merck, Darmstadt, Germany) and transferred into a stainless steel tank. From the pressurized tank the solution was sprayed into liquid nitrogen. In a cold room below -25°C , the resulting ice was ground with an electric mill, passed through a test sieve with a mesh size of 0.5 mm, and stored at least overnight in 1 L glass bottles covered with aluminum foil.

The experimental set-up was similar to previously performed photolysis experiments [27,39]. A mercury-arc lamp (Oriental Instrument, Stratford, CT) with a maximum power input of about 1000 W was used as the light source. For the experiments the power input was reduced to 500 W. A 10 cm long liquid-filter filled with Milli-Q water was directly coupled to the output of the lamp housing condenser to absorb the infrared radiation. The transmittance of the water filter was about 80% between the wavelengths of 250 and 700 nm [27]. An additional 10 cm long cylindrical extension made of white synthetic material was fixed to the end of the liquid-filter. The snow samples were filled into cylindrical 1 cm long Teflon cells, equipped with quartz windows. The reaction cells were easily attached to the end of the extension, which was equipped with a flange with an inner-diameter equal to the outer-diameter of the cells. The snow sample was completely illuminated by the light beam since the liquid-filter, the cylindrical extension, and the reaction cells had the same inner-diameter of 4.6 cm (Fig. 1).

The experiment was installed inside an opening of a freezer so that two-thirds of the extension and the entire reaction cell were located inside the freezer, which was regulated to a temperature of -31 to -30°C . Before each experiment, the filled cell was stored several hours in the freezer to assure that the temperature of the snow was in equilibrium with the freezer's temperature. To start and end the single experiments, the cell was either placed inside or removed from the flange of the extension reaching through a second, normally closed opening of the freezer.

The NO_3^- and NO_2^- concentrations in the snow were determined before and after each experiment. When filling the cell for a new experiment, a sample of the same batch of snow was kept in an airtight bottle. After the experiment, the snow was

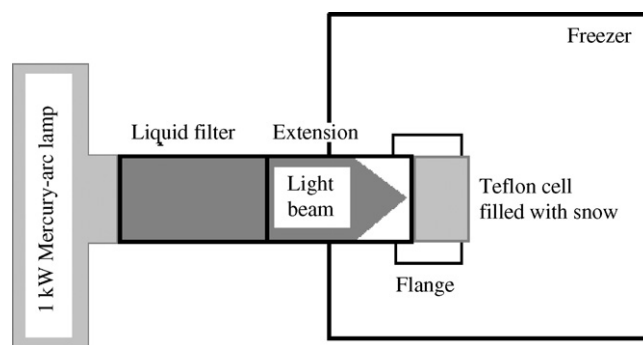


Fig. 1. Experimental system of the photolysis experiments.

Table 1

Measured initial concentrations of NO_3^- and NO_2^- in the snow samples, calculated liquid QLL fraction, and corresponding calculated initial concentrations in the QLL

Batch	Temperature ($^{\circ}\text{C}$)	$C_{\text{bulk}}^{\text{a}}$ (μM)		$\varphi_{\text{H}_2\text{O}}^{\text{b}}$ ($\times 10^{-5}$)	C_{T}^{c} (mM)	
		$[\text{NO}_3^-]_0$	$[\text{NO}_2^-]_0$		$[\text{NO}_3^-]_0$	$[\text{NO}_2^-]_0$
1	-31	10.84	0.161	3.42	317	4.71
2	-31	9.97	0.185	3.29	303	5.62
3	-30	1.66	3.28	2.33	71.2	141
4	-31	0.757	11.72	3.64	20.8	322
^d	-20	12.55	0.084	4.65	270	1.80
^e	-20	4.4	0	1.94	230	0

^a Concentrations measured in the melted snow samples.

^b Liquid fraction calculated using Eq. (4).

^c QLL concentrations calculated using Eq. (3).

^d Concentrations and QLL fraction calculated for the experiments presented by Jacobi et al. [27].

^e Concentrations and QLL fraction calculated for average NO_3^- concentration measured in surface snow during the summer of 2000 at Summit [11].

completely removed from the cell and filled into a second airtight bottle. The bottles were stored in the dark at -20°C and the melted samples were analyzed using an ion chromatography system [27]. The system was always calibrated with a range of standard solutions and Milli-Q water before and after the analysis of the samples. The analytical error was $\pm 3 \times 10^{-8}$ M for NO_3^- and $\pm 4 \times 10^{-8}$ M for NO_2^- or $\pm 10\%$, whichever is larger.

3. Results

Photolysis experiments with four different batches of artificial snow were performed with varying initial concentrations of NO_3^- and NO_2^- (Table 1). Batches 1 and 2 contained the highest initial NO_3^- concentrations ($\sim 10^{-5}$ M) in the presence of almost negligible NO_2^- amounts. Irradiation caused a logarithmic decomposition of NO_3^- during the experiments (Fig. 2a). In the same experiments NO_2^- was first produced reaching a concentration maximum in the experiments lasting around 30 min. Thereafter, NO_2^- decreased after longer irradiation periods. However, the behavior of both compounds changed with elevated initial NO_2^- concentrations. The results of the batches 3 and 4 demonstrate that with higher initial NO_2^- concentrations the drop in the NO_3^- concentrations was delayed or even absent (Fig. 2b and c). Increasing the NO_2^- concentration to 1.2×10^{-5} M even caused a significant production of NO_3^- (Fig. 2c). On the other hand, the NO_2^- concentrations showed a steady decrease in the batches 3 and 4 with increasing irradiation times.

4. Discussion

4.1. Development of a reaction mechanism for the transformation of NO_3^- and NO_2^- in snow

The experimental results cannot be reconciled with the following previously proposed reaction sequence [27]:



Such a reaction sequence is in conflict with the observation of the formation of NO_3^- in the experiments with significant initial NO_2^- concentrations. Additional reactions are needed to describe the experimental data. According to the known reaction

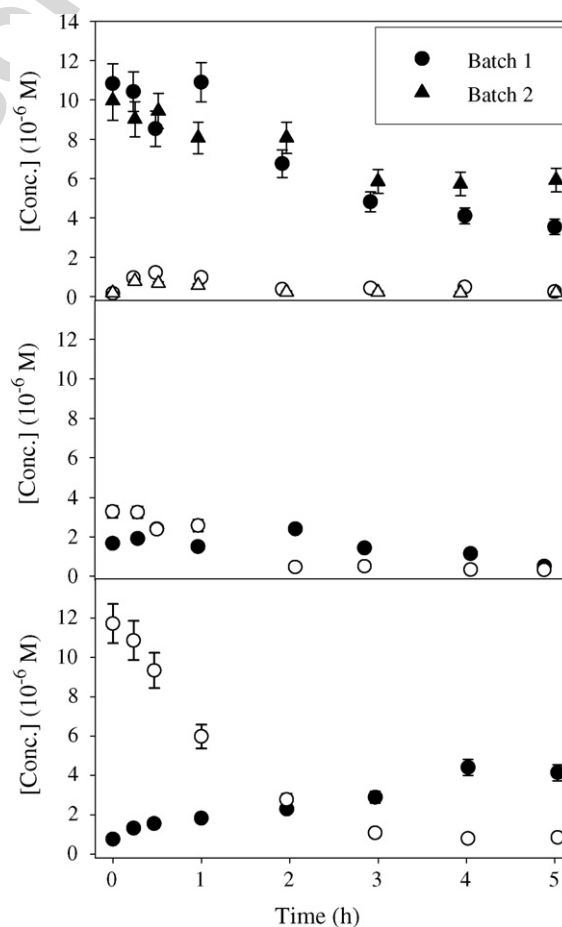
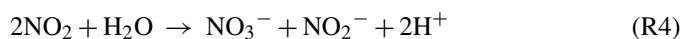


Fig. 2. Plots of the NO_3^- (filled symbols) and NO_2^- concentrations (open symbols) measured in the melted snow after each photolysis experiment vs. the duration of the experiments: (a) batches 1 and 2, (b) batch 3, and (c) batch 4 (initial concentrations see Table 1). Error bars represent analytical errors. If no error bar is visible, the errors are smaller than the size of the symbols.

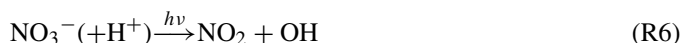
mechanism in the aqueous phase [33] NO_2^- can be oxidized to NO_3^- via the formation of nitrogen dioxide (NO_2). Using NO_2^- as a precursor, NO_2 formation can occur through two different pathways: attack by OH (R1) and photolysis of NO_2^- (R2) with the subsequent oxidation of NO by dissolved oxygen (R3):



In the reaction (R2) an oxide radical ion (O^-) is first generated, which immediately adds a proton to yield OH radicals [40]. NO_2 can subsequently be oxidized to NO_3^- either by the formation of the dimer N_2O_4 followed by hydrolysis (R4) [25] or by the attack of an OH radical (R5):



Two reaction channels are possible during the photolysis of NO_3^- : either the formation of NO_2 (R6) or NO_2^- (R7):



An additional product of reaction (R7) is the oxygen atom (O). It can react with dissolved oxygen to produce ozone (R8) and with NO_3^- producing additional NO_2^- (R9):



Table 2
Reactions included in the mechanism for the photochemical transformation of NO_3^- and NO_2^- in snow

Reaction no.	Reaction rates ^a			Reference
	$T = -31^\circ\text{C}$	$T = -20^\circ\text{C}$	Summit ^b	
$\text{OH} + \text{NO}_2^- \rightarrow \text{NO}_2 + \text{OH}^-$ (R1)	$1 \times 10^{10} \text{M}^{-1} \text{s}^{-1}$	$1 \times 10^{10} \text{M}^{-1} \text{s}^{-1}$	$1 \times 10^{10} \text{M}^{-1} \text{s}^{-1}$	[41]
$(\text{R2}) \text{NO}_2^- (+\text{H}^+) \xrightarrow{h\nu} \text{NO} + \text{OH}$	$3 \times 10^{-3} \text{s}^{-1\text{c}}$	$8.4 \times 10^{-3} \text{s}^{-1\text{d}}$	$2.5 \times 10^{-5} \text{s}^{-1}$	This work
$2\text{NO} + \text{O}_2 \rightarrow 2\text{NO}_2$ (R3)	$360 \text{M}^{-1} \text{s}^{-1\text{e}}$	$420 \text{M}^{-1} \text{s}^{-1\text{e}}$	$420 \text{M}^{-1} \text{s}^{-1\text{e}}$	[42]
$2\text{NO}_2 + \text{H}_2\text{O} \rightarrow \text{NO}_3^- + \text{NO}_2^- + 2\text{H}^+$ (R4)	$1 \times 10^7 \text{M}^{-1} \text{s}^{-1}$	$1.4 \times 10^7 \text{M}^{-1} \text{s}^{-1}$	$1.4 \times 10^7 \text{M}^{-1} \text{s}^{-1}$	[43]
$\text{NO}_2 + \text{OH} \rightarrow \text{H}^+ + \text{NO}_3^-$ (R5)	$5 \times 10^9 \text{M}^{-1} \text{s}^{-1}$	$5 \times 10^9 \text{M}^{-1} \text{s}^{-1}$	$5 \times 10^9 \text{M}^{-1} \text{s}^{-1}$	[44]
$(\text{R6}) \text{NO}_3^- (+\text{H}^+) \xrightarrow{h\nu} \text{NO}_2 + \text{OH}$	$1 \times 10^{-4} \text{s}^{-1\text{c}}$	$2.8 \times 10^{-4} \text{s}^{-1\text{d}}$	$8.3 \times 10^{-7} \text{s}^{-1}$	This work
$(\text{R7}) \text{NO}_3^- \xrightarrow{h\nu} \text{NO}_2^- + \text{O}$	$2 \times 10^{-5} \text{s}^{-1\text{c}}$	$5.6 \times 10^{-5} \text{s}^{-1\text{d}}$	$1.7 \times 10^{-7} \text{s}^{-1}$	This work
$\text{O} + \text{O}_2 \rightarrow \text{O}_3$ (R8)	$1.2 \times 10^6 \text{s}^{-1\text{e}}$	$1.2 \times 10^6 \text{s}^{-1\text{e}}$	$1.2 \times 10^6 \text{s}^{-1\text{e}}$	[45]
$\text{NO}_3^- + \text{O} \rightarrow \text{NO}_2^- + \text{O}_2$ (R9)	$2 \times 10^8 \text{M}^{-1} \text{s}^{-1}$	$2 \times 10^8 \text{M}^{-1} \text{s}^{-1}$	$2 \times 10^8 \text{M}^{-1} \text{s}^{-1}$	[19]
$\text{NO} + \text{OH} \rightarrow \text{H}^+ + \text{NO}_2^-$ (R10)	$2 \times 10^{10} \text{M}^{-1} \text{s}^{-1}$	$2 \times 10^{10} \text{M}^{-1} \text{s}^{-1}$	$2 \times 10^{10} \text{M}^{-1} \text{s}^{-1}$	[46]
$\text{NO} + \text{NO}_2 + \text{H}_2\text{O} \rightarrow 2\text{NO}_2^- + 2\text{H}^+$ (R11)	$3 \times 10^8 \text{M}^{-1} \text{s}^{-1}$	$3 \times 10^8 \text{M}^{-1} \text{s}^{-1}$	$3 \times 10^8 \text{M}^{-1} \text{s}^{-1}$	[47]
$(\text{R12}) \text{NO}_2 \xrightarrow{h\nu} \text{NO} + \text{O}$	1s^{-1}	2.8s^{-1}	$8.3 \times 10^{-3} \text{s}^{-1}$	Estimated
$\text{NO} \rightarrow \text{NO}_{\text{gas}}$ (R13)	$45 \text{s}^{-1\text{c}}$	$57 \text{s}^{-1\text{d}}$	57s^{-1}	This work
$\text{NO}_2 \rightarrow \text{NO}_{2\text{gas}}$ (R14)	$3 \text{s}^{-1\text{c}}$	$9.7 \text{s}^{-1\text{d}}$	9.7s^{-1}	This work

^a Reaction rates were taken from kinetic data determined in the aqueous liquid phase. If temperature-dependent rate constants were available, reaction rates were extrapolated to sub-freezing temperatures.

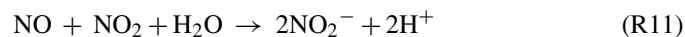
^b Reaction rates estimated for conditions at GEO Summit in summer 2000.

^c Reaction rates determined for experiments here, performed at -31°C .

^d Reaction rates determined for previously published experiments [27], performed at -20°C .

^e First- and second-order rate constants calculated with $[\text{O}_2] = 0.3 \mu\text{M}$ [19].

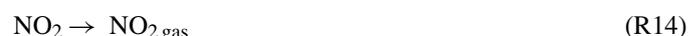
Additional reactions leading to the formation of NO_2^- is the reaction of OH with NO (R10) and the reaction of NO with NO_2 with the subsequent hydrolysis of N_2O_3 (R11):



Due to the experimental conditions, we also need to take into account the photolysis of NO_2 to NO in the snow (R12):



Finally, due to the low solubility the nitrogen oxides are transferred to the gas phase (R13) and (R14):



The full reaction mechanism used for the analysis of the experimental data is shown in Table 2. We used aqueous phase kinetic data for the rate constants of the bimolecular reactions. If temperature-dependent rate constants were available, they were extrapolated to sub-freezing temperatures (Table 2).

The rate constants of the NO_2^- and NO_3^- photolysis reactions (R2), (R6), and (R7) and the rates for the phase transfer reactions of NO and NO_2 ((R13) and (R14)), were derived by fitting the experimental and calculated concentration–time curves using the commercial FACSIMILE software. For the fitting procedure we used the measured NO_3^- and NO_2^- concentrations and gas phase $\text{NO}_{x\text{gas}}$ concentrations. Since $\text{NO}_{x\text{gas}}$ was not directly measured, we calculated the gas phase concentration as the difference from the measured ($[\text{NO}_3^-]$, $[\text{NO}_2^-]$) to the initial NO_3^- and NO_2^- concentrations ($[\text{NO}_3^-]_0$, $[\text{NO}_2^-]_0$) in

the snow:

$$[\text{NO}_{x\text{gas}}] = [\text{NO}_3^-]_0 + [\text{NO}_2^-]_0 - ([\text{NO}_3^-] + [\text{NO}_2^-]) \quad (1)$$

Although the NO_x transfer rates k_{R13} and k_{R14} varied, we always used a fixed ratio of $k_{R13}/k_{R14} = 15$ since the extrapolated Henry's law constants of both compounds at $T = 31^\circ\text{C}$ differ by a factor of 15 [48]. This assumption is in agreement with previous laboratory experiments suggesting that NO_2 is more strongly bound than NO to the ice [26].

Several laboratory studies have provided evidence that the photolysis of nitrate and the subsequent reactions in ice and snow take place in a so-called quasi-liquid layer (QLL) on the surface of ice crystals [19,20,22,23]. Although the properties of the QLL are not well established, it is now well known that at temperatures close to the melting point and/or in the presence of impurities, the QLL shows a strongly enhanced disorder compared to the highly ordered interior of the ice crystal (e.g. [49–53]). Nevertheless, the QLL is always restricted to a limited number of layers of water molecules. If all reactions in the condensed phase take place in this much smaller volume, the calculations must be performed using significantly higher concentrations. Cho et al. [51] performed NMR spectroscopy to determine the fraction of water in the QLL $\varphi_{\text{H}_2\text{O}}$ as a function of temperature T and the total solute concentration in the QLL C_T^0 . They obtained the following equation (2):

$$\varphi_{\text{H}_2\text{O}}(T) = \frac{m_{\text{H}_2\text{O}}RT_f}{1000H_f^0} \frac{T}{T - T_f} C_T^0 \quad (2)$$

Here, $m_{\text{H}_2\text{O}}$ is the molecular weight of water, R the gas constant, H_f^0 the melting enthalpy of water, and T_f is the freezing temperature of water.

The concentration in the QLL is not directly available for our experiments since the analysis of the melted snow samples yields only the bulk snow concentrations. Nevertheless, these can be translated into the QLL concentrations if we assume that all impurities are located in the QLL. In that case, we can relate the bulk concentration C_{bulk} to the QLL concentrations C_T^0 by the following Eq. (3):

$$C_{\text{bulk}} = \varphi_{\text{H}_2\text{O}}(T) C_T^0 \quad (3)$$

Substituting this expression into Eq. (2), we find

$$\varphi_{\text{H}_2\text{O}}(T) = \sqrt{\frac{m_{\text{H}_2\text{O}}RT_f}{1000H_f^0} \frac{T}{T - T_f} C_{\text{bulk}}} \quad (4)$$

The QLL fractions ($\varphi_{\text{H}_2\text{O}}$ listed in Table 1) were obtained with Eq. (4) for the initial conditions of the four different snow batches. Applying Eq. (3), $\varphi_{\text{H}_2\text{O}}$ was subsequently used to calculate QLL concentrations of NO_3^- and NO_2^- for the experiments performed with the four snow batches as shown in Table 1 for the initial concentrations. Fig. 3 shows the results of all four batches transformed into QLL concentration and also the gas phase NO_x concentrations as calculated from the differences between actual and initial NO_3^- and NO_2^- concentrations in the snow according to Eq. (1). For an easier comparison the $\text{NO}_{x\text{gas}}$ concentrations are also plotted in M units like the QLL concentrations.

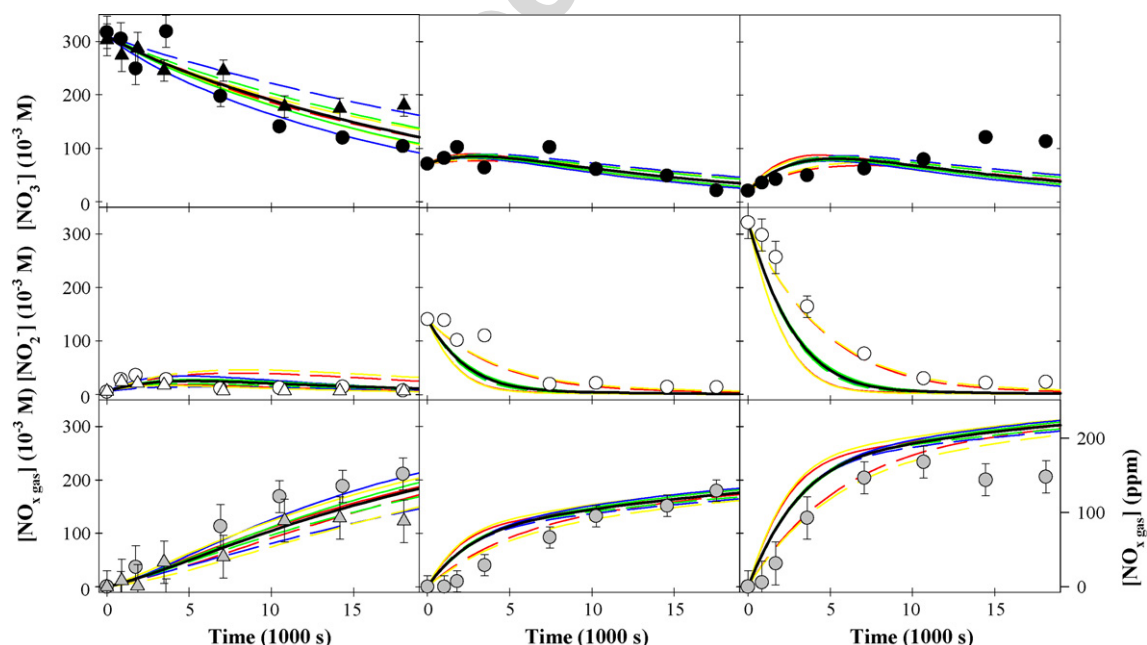


Fig. 3. Comparison of experimental and calculated concentration-time-profiles for NO_3^- (top) and NO_2^- concentrations (middle) in the QLL and $\text{NO}_{x\text{gas}}$ in the gas phase (bottom) for the snow batches 1 and 2 (left), batch 3 (middle), and batch 4 (right). On the left axis the NO_x concentration is shown in M as calculated according to Eq. (1) as the deficit of NO_3^- and NO_2^- in the snow samples. On the right axis the NO_x concentrations are transformed into gas phase mixing ratios taking into account the mass of the snow and the gas phase volume in the cell. The black line represents calculated profiles using the optimum rate constants (see text). Colored lines represent calculated profiles with single rate constants varying by +50% (full lines) and -50% (dashed lines) with variation of k_{R2} : red, k_{R7} : blue, k_{R6} : green, and k_{R13} and k_{R14} : yellow. Error bars for NO_3^- and NO_2^- represent analytical errors. The error of the gas phase NO_x is calculated from the analytical errors of NO_3^- and NO_2^- using error propagation. If no error bar is visible, the errors are smaller than the size of the symbols.

A common best-fit was determined using the QLL concentrations of all four batches of snow shown in Fig. 3. Best agreement between the experiments and the calculated concentration–time-profiles were found with the following rate constants for the photolytic reactions of NO_2^- and NO_3^- : $k_{R2} = 3 \times 10^{-3} \text{ s}^{-1}$, $k_{R6} = 1 \times 10^{-4} \text{ s}^{-1}$, and $k_{R7} = 2 \times 10^{-5} \text{ s}^{-1}$. Thus, in our experiments the photolysis of NO_2^- occurred a factor of ~ 25 faster than the overall photolysis of NO_3^- . The two different reaction channels for the NO_3^- photolysis, generating NO_2 (R6) and NO_2^- (R7), contributed 83% and 17%, respectively, which is in reasonable agreement with previous studies in fluid and frozen media [19,21,22,33].

In addition, the optimum transfer rates for NO and NO_2 were determined to be on the order of $k_{R13} = 45 \text{ s}^{-1}$ and $k_{R14} = 3 \text{ s}^{-1}$, respectively. Fig. 3 shows a comparison of the time series of experimental and modeled QLL concentrations obtained with the optimum rate constants. The sensitivities of the calculated concentrations to changes in the rate constants were tested. The reaction rate constants k_{R2} , k_{R6} , and k_{R7} and the transfer constants k_{R13} and k_{R14} were separately changed by a factor of 2 (the ratio of k_{R13} to k_{R14} remained constant). The results of these sensitivity studies are also shown in Fig. 3.

In general, the calculated concentrations are in good agreement with the experimental data. The deviations between modeled and experimental data are in the same range as the variability of the results for the two different snow batches 1 and 2 with comparable initial concentrations. Applying the mechanism, we are able to reproduce the reduction in NO_3^- and NO_2^- if high initial concentrations of either compound were present in the snow. The mechanism also captures the transformation of NO_2^- to NO_3^- observed in the batches 3 and 4 (Fig. 3). The quick release of nitrogen oxides to the gas phase is also well reproduced by the model. However, the NO_2^- drop occurs somewhat faster in the model compared to the experiments performed with the batches 2 and 3. Better agreement is obtained if either the rate constant k_{R2} for the photolysis of NO_2^- (dashed red line) or the transfer rates k_{R13} and k_{R14} of NO and NO_2 (dashed yellow line) were reduced by 50% (Fig. 3). However, these higher rates would lead to a much worse agreement with the results of the batches 1 and 2 with small initial NO_2^- concentrations. Therefore, the proposed rate constants constitute a compromise for all four experiments. The gas phase NO_x concentrations are also sensitive to the rate constants k_{R2} , k_{R13} , and k_{R14} . Similar to NO_2^- , the agreement between modeled and measured NO_x becomes better with higher rate constants for the batches 3 and 4 and worse for the batches 1 and 2. In contrast, the calculated NO_3^- concentrations are most sensitive to the photolysis rate constants k_{R6} and k_{R7} of NO_3^- .

4.2. Comparison with previous laboratory data

Jacobi et al. [27] previously presented results of similar experiments regarding the photolytic decomposition of nitrate in snow. Here, we apply the newly developed reaction mechanism to reproduce the experimental data. However, due to the different experimental conditions the rate constants need to be adjusted. First, the distance between the reaction cell and the lamp was

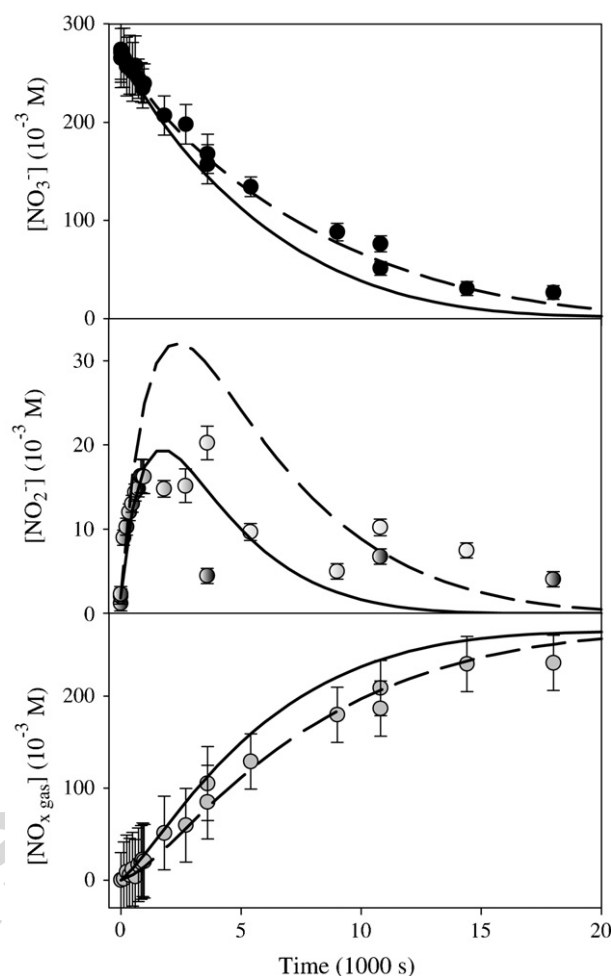


Fig. 4. Comparison of experimental and calculated concentration–time-profiles for NO_3^- (top) and NO_2^- concentrations (middle) in the QLL and NO_x in the gas phase (bottom) for previous experiments [27] performed at -20°C . The NO_x concentrations are calculated according to Eq. (1). The dashed line represents calculated profiles with all photolysis rates multiplied by 2.8 (see text). The full lines represent calculated profiles with increased photolysis rates and increased transfer rates for NO and NO_2 as summarized in Table 2 (see text). Error bars for NO_3^- and NO_2^- represent analytical errors. The error of the gas phase NO_x is calculated from the analytical errors of NO_3^- and NO_2^- using error propagation.

smaller in the previous experimental set-up (16 cm), compared to the current set-up (27 cm). These different distances caused higher radiation intensities per area by a factor of 2.8 since the intensity decreases with the square of the distances from the light source. Therefore, we increased all photolysis rates (k_{R2} , k_{R6} , k_{R7} , and k_{R12}) by a factor of 2.8 (Table 2). Second, the previous experiments were performed at a higher temperature of -20°C [27]. We adjusted the rate constants k_{R3} and k_{R4} using the temperature dependencies of the rate constants reported in the literature [42,43]. However, the changes are smaller ($\leq 40\%$) than the assumed error of the fitted photolysis rate constants (Table 2). Fig. 4 shows calculated concentration–time-profiles with the increased photolysis and reaction rates. Moreover, the temperature also influences the phase transfer. Using, again, Henry's law constants as a reference, we find that the con-

stant for NO decreases from $5.6 \times 10^{-3} \text{ M atm}^{-1}$ at -31°C to $4.4 \times 10^{-3} \text{ M atm}^{-1}$ at -20°C [48]. The decrease is even more pronounced for NO_2 from $8.4 \times 10^{-2} \text{ M atm}^{-1}$ at -31°C to $2.6 \times 10^{-2} \text{ M atm}^{-1}$ at -20°C [48]. Therefore, we enhanced the transfer constants similarly (Table 2), reducing the ratio of k_{R13} to k_{R14} from 15 at -31°C to smaller than 6 at -20°C . Calculated concentration–time–profiles with the increased transfer rates are also shown in Fig. 4. The comparison with the experimental data shows that the agreement for NO_2^- is much improved with the higher transfer rates. With the lower transfer rates the maximum NO_2^- concentration is approximately 50% higher than the highest NO_2^- concentrations determined in any of the experiments. The higher transfer rates lead to maximum NO_2^- concentrations, which fall well in the range of the observed concentrations. On the other hand, the faster transfer leads to slightly overestimated values for the NO_x concentrations in the gas phase and slightly underestimated values for NO_3^- . The discrepancies become larger for experiments lasting longer than 5000 s (≈ 1.4 h) and might be due to the equilibrium of NO and NO_2 between the gas phase and the QLL. If the gas phase concentrations are sufficiently high a transfer back from the gas phase to the QLL becomes possible. This could explain the slightly lower gas phase and slightly higher NO_3^- concentrations observed in the experiments.

4.3. Comparison with field data: NO_x emissions

Having established a mechanism for the photochemical transformation of nitrogen containing compounds in snow, we can apply this mechanism to previous field observations. The most comprehensive data set, which provides the needed input information, is currently available from measurements performed at the Greenland environmental observatory summit (GEO Summit) on top of the Greenland ice sheet (72.6°N , 38.5°W , 3200 m elevation) in the summer of the year 2000. For example, nitrate photolysis rate coefficients were directly measured in the snow using chemical actinometry [10]. Average values for midday exposures were on the order of 10^{-6} s^{-1} at depths smaller than 5 cm. Therefore, we decreased the rate coefficients k_{R6} and k_{R7} so that the sum of both photolysis rates gives a value of 10^{-6} s^{-1} (Table 2). Accordingly, we also reduced the photolysis rates k_{R2} of NO_2^- and k_{R12} of NO_2 by the same factor, since this reaction will also be much slower under natural conditions. The reported snow temperatures for Summit varied between -4°C at the surface and -21°C at a depth of 15 cm for the period of the photolysis rate measurements [10]. Although the experimental temperature of -20°C is close to the lower limit of the

temperature in the natural snow, we did not attempt to adjust the rate constants further. NO_3^- in surface-snow at Summit shows considerable short-term variability [54]. We used an average concentration of $3 \mu\text{M}$ as reported by Dibb et al. [54] for the initial concentration in our calculations.

The rate constants and the initial calculated QLL concentration of NO_3^- are summarized in Tables 1 and 2. QLL concentrations and gas phase NO_x production rates simulated after reaction times of 2 and 4 h are shown in Table 3. Fig. 5 shows a concentration and flux diagram for conditions after reaction times of 2 h. The diagram shows the conversion of the nitrogen compounds in the QLL and the transfer to the gas phase.

For the applied conditions the model predicts that the photochemical transformation of NO_3^- occurs very slowly. For example, after a reaction time of 4 h the NO_3^- concentrations are apparently reduced by less than 1% compared to the initial NO_3^- concentration, although the observed photolysis rate suggests that in such a period almost 1.4% of the initial NO_3^- would have been photolyzed. Obviously, the recycling of NO_3^- via the oxidation of NO_2 contributes to the slower apparent NO_3^- decrease. Fig. 5 shows that after a reaction time of 2 h the total sink strength of NO_3^- via the photolysis reactions (R6) and (R7) and the reaction with the O atom (R9) assumes a value of $2.7 \times 10^{-7} \text{ M s}^{-1}$. However, the net destruction of NO_3^- is reduced by more than 40% due to the oxidation of NO_2 to NO_3^- mainly via the reaction with OH (R5).

NO_2^- concentrations in the QLL increase quickly and reach maximum values of $5.9 \times 10^{-9} \text{ M}$ after just several seconds before they decrease slowly. Translating the QLL concentrations into bulk snow concentrations using the QLL fraction (Table 2) leads to extremely small NO_2^- concentrations of less than $2 \times 10^{-13} \text{ M}$ in the snow. Such concentrations are far beyond the detection limit of currently used chemical snow analysis methods (e.g. [55–57]). Nevertheless, NO_2^- concentrations up to $1.8 \times 10^{-7} \text{ M}$ in arctic snow samples were reported at depths of 25 cm, while the concentrations remained below $7 \times 10^{-8} \text{ M}$ at the surface [58]. A photochemical generation of such high NO_2^- concentrations is only possible with radiation intensities as high as in our laboratory experiments (Fig. 2). Since these intensities are orders of magnitudes higher than the intensity of the solar radiation at the Earth's surface [39], additional sources of NO_2^- must be invoked to explain the NO_2^- observations. Such sources could be the dry deposition of HONO or the precipitation of fresh snow with higher NO_2^- concentrations due to the scavenging of gas phase HONO. The destruction of NO_2^- is dominated by the reaction with OH (R1), while the photolysis is a negligible sink of NO_2^- under natural conditions. This

Table 3

Calculated QLL concentrations and gas phase NO_x production rates calculated for conditions at Summit observed in the summer of 2000

Time ^a (h)	$[\text{NO}_3^-]$ (M)	$[\text{NO}_2^-]$ ($\times 10^{-9}$ M)	$[\text{NO}_2]$ ($\times 10^{-8}$ M)	$[\text{NO}]$ ($\times 10^{-12}$ M)	$[\text{OH}]$ ($\times 10^{-9}$ M)	$P(\text{NO}_2)^b$ ($\times 10^{12}$ molecules s^{-1})	$P(\text{NO})^b$ ($\times 10^8$ molecules s^{-1})
2	0.229	5.84	1.59	1.48	1.38	1.80	9.83
4	0.228	5.81	1.58	1.47	1.38	1.79	9.78

^a Time after the initiation of the calculations.

^b Production rates of gas phase NO_2 and NO calculated for 1 L of irradiated snow.

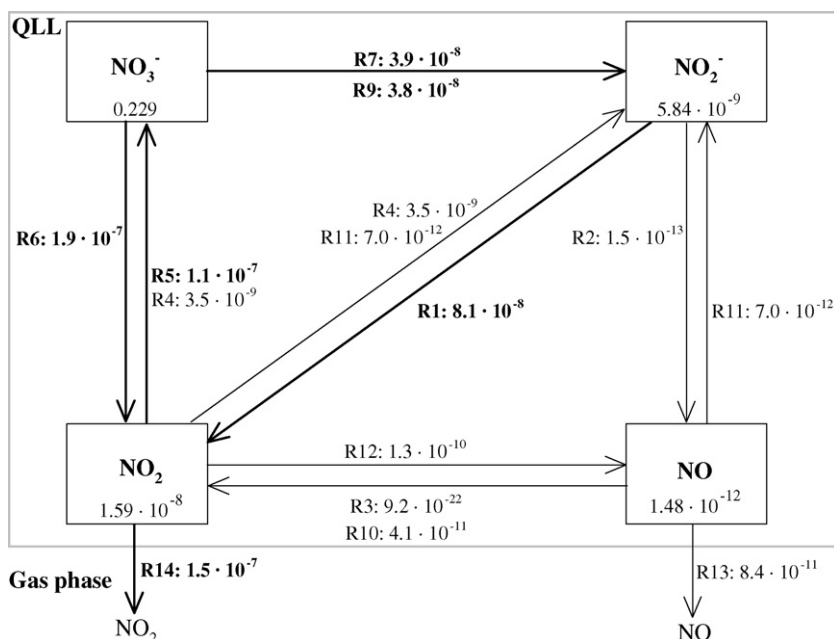


Fig. 5. Concentration and flux diagram for the photolysis of NO_3^- in the QLL of the surface snow calculated for typical conditions at Summit in the year 2000. The numbers are computed for $t=2$ h after the initiation of the calculations. Concentrations are given in M, fluxes for single reactions (see Table 2 for reaction numbers) are given in M s^{-1} . For example, the flux of NO_2 to the gas phase of $1.5 \times 10^{-7} \text{ M s}^{-1}$ corresponds to an emission rate of 1.8×10^{12} molecules s^{-1} for 1 L of snow (see Table 3). Thick arrows represent dominant conversion pathways with fluxes larger than $3 \times 10^{-8} \text{ M s}^{-1}$.

is in agreement with previous laboratory studies of the NO_3^- photolysis in the presence of radical scavengers. For example, Honrath et al. [18] observed a much smaller NO_2 production in the presence of OH scavengers. Similarly, Dubowski et al. [20] reported increased yields of NO_2^- if they added an OH radical scavenger like formate to their ice samples. Both observations indicate that the conversion of NO_2^- to NO_2 ceased if OH were significantly removed.

The model results demonstrate that the release of NO_x is dominated by NO_2 (Fig. 5). NO_2 is generated either directly by the photolysis of NO_3^- (R6) or via the formation of NO_2^- from NO_3^- by the reactions (R7) and (R9) and the subsequent reaction of NO_2^- with OH (R1). The main sinks of NO_2 are the oxidation to NO_3^- by the OH radical (R5) and the transfer to the gas phase (R14). Since both pathways are almost equal, a significant fraction of the NO_2 produced in the QLL undergoes chemical reactions prior to the release to the gas phase. This was also observed in previous laboratory experiments using thin ice films [25,26]. However, our model calculations indicate that for natural conditions the reaction with the OH radical (R5) is far more important than the hydrolysis of the NO_2 dimer (R4) as suggested for the laboratory experiments [25].

Compared to NO_2 , NO concentrations as well as the NO transfer to the gas phase are orders of magnitude smaller. Therefore, NO in the QLL plays probably a negligible role for the photochemical transformation of nitrogen containing compounds as well as the release of NO_x to the firm air. The ratio of the NO_2 to NO fluxes to the gas phase assumes a value of approximately 1800 (Table 3) and remains constant for several hours in the simulations.

Similarly, previous studies of the NO_3^- photolysis using natural or artificial snow samples [3,5,18,21] or thin ice layers [23,26] have also indicated that the NO_x flux to the gas phase was dominated by NO_2 , although in most cases the emission of NO was not negligible with ratios of the NO_2 to NO production rates between 2 and 8 in the snow experiments [5,18,21] and ratios between 10 and 23 in the experiments with the ice films [23,26]. However, the formation of NO possibly indicates further reactions in the gas phase like the photolysis of NO_2 and HONO, which can also lead to the formation of NO . At least in the snow experiments with long residence times of the sampled air in the illuminated zone on the order of minutes [5,18,21], these gas phase reactions must be considered as discussed by Cotter et al. [21].

The calculated NO_2 production rate amounts to 1.8×10^{12} molecules s^{-1} in 1 L of irradiated snow. Such a production rate translates into a NO_2 flux of 5.4×10^{12} molecules $\text{m}^{-2} \text{s}^{-1}$ taking into account a snow layer with a depth of 1 cm and a density of 0.3 g cm^{-3} . This flux must be considered as representative for conditions at noon due to the selected photolysis rates for the model run. We can compare this value to NO_x fluxes measured above the snow surface at Summit in 2000. According to Honrath et al. [11], the NO_x emissions were correlated with the solar radiation intensities with two thirds of the NO_x fluxes observed around noon falling in a range between 2 and 11×10^{12} molecules $\text{m}^{-2} \text{s}^{-1}$ [11]. The agreement between the modeled and observed NO_x fluxes is excellent if we assume that the NO_x release to the atmosphere is determined by the top 1 or 2 cm of the snow. However, it is very likely that a thicker snow layer contributes to the photochemical production of NO_x .

since the penetration depth of the solar radiation into the snow is deeper than just a few centimeters. For example, in the UV and visible range Peterson et al. [59] found that in the same snowpack at Summit approximately 10% of the incident radiation at the snow surface is transmitted to a depth of 10 cm. Since the NO_x fluxes were measured above the snow surface, they represent only the fraction of NO_x , which actually escaped from the so-called firn air, which is the interstitial air of the surface snow. The NO_x production rates in the snow can be significantly higher if a large fraction is oxidized in the firn air and re-deposited to the snow before it is released to the atmosphere. An indication of high NO_x production rates is for example the extremely high NO_x concentration in the firn air also measured at Summit [14].

The modification of the reaction mechanism developed for the laboratory experiments to conditions in the natural snowpack is accompanied by rather high uncertainties. These mainly arise from the vastly different emission spectrum of the lamp compared to the spectrum of the solar radiation [27]. The irradiation emitted by the lamp shows a strong band in the UV range, which overlaps with the absorption spectrum of NO_3^- . However, such a band is absent in the solar radiation. Therefore, the ratio of the photolysis rates of NO_2^- and NO_3^- is probably larger in the natural snowpack compared to the laboratory experiments. To account for this effect, we performed additional model runs with fixed NO_3^- photolysis rates k_{R6} and k_{R7} determined by the rates measured at Summit as described above, but with a NO_2^- photolysis rate k_{R2} increased by a factor of 10 and 100, respectively. In both cases the effects on the calculated QLL concentrations are small. The largest effects are obtained for the modeled NO concentrations, which increase by less than 1% with k_{R2} multiplied by 10 and by less than 11% with k_{R2} multiplied by 100. The changes of all other concentrations are smaller than 1%. The reason for these small changes is the minor importance of the NO_2^- photolysis (R2) as displayed in Fig. 5. The production rate of NO by this reaction is almost three orders of magnitude smaller than by the photolysis of NO_2 (R12). Therefore, multiplying k_{R2} by a factor of 100 increases the total NO production rate only by a few percent. Such a small increase in the NO production has only a slight impact on the modeled NO concentrations and the ratio of the NO and NO_2 concentrations. Although additional experiments are needed to determine the exact photolysis rate constants for natural conditions, we do not expect drastic changes for instance in the ratio of the NO_2 to NO concentrations and fluxes to the gas phase.

4.4. HONO production in the surface snowpack

Besides the emission of NO_x , upward fluxes of HONO from the surface snow to the atmosphere have been reported for the Canadian Arctic [8] and Summit [11]. Although the gas phase HONO production is currently not incorporated into the mechanism, we can use the computed concentrations to determine if a sufficiently high production of HONO can occur in the QLL to explain the measured emissions. The HONO transfer to the gas phase depends on several parameters like the NO_2^- concentration in the QLL, the pH of the QLL, and the HONO phase transfer rate. Since we did not attempt to compute the proton

concentrations directly, we will compare the ratio of the gas phase HONO to NO_2 production rates and discuss the impact of the pH on this ratio.

HONO is a moderately weak acid with a dissociation constant pK_a reported in the literature in the range from 2.3 to 5.2 [60]. Here, we use an extrapolated pK_a of 3.7 at a temperature of -20°C [47]. Thus, 99% of the NO_2^- would be present at HONO in the QLL at a pH of 1.7. However, Table 3 demonstrates that the NO_2^- concentrations are always lower than the NO_2 concentrations by a factor of approximately 3. Even with a full conversion of NO_2^- to HONO at low pH values, the HONO concentrations will remain smaller than the NO_2 concentrations in the QLL. Nevertheless, the HONO flux to the gas phase could be comparable to the NO_2 flux if the lower concentration is compensated by a higher transfer rate. Similarly to the case of NO and NO_2 , we calculate the phase transfer rate relative to the Henry's law constant. Due to the much higher solubility of HONO, the Henry's law constant is significantly higher compared to the values for the nitrogen oxides. Using temperature-dependent parameters [48], we obtain a value of 930 M atm^{-1} extrapolated to -20°C for HONO. Since this number is a factor of 3.6×10^4 higher than the Henry's law constant of NO_2 at the same temperature, we assume that the phase transfer rate of HONO is significantly smaller compared to the transfer of NO_2 . In combination with the lower transfer rate, we conclude that the HONO transfer from the QLL is orders of magnitude smaller than the parallel NO_x transfer. Thus, the NO_3^- photolysis in snow is a negligible direct source of HONO in contrast to previous suggestions (e.g. [37]). However, such small HONO production rates can explain neither the enhanced HONO concentrations measured in the firn air [14], nor the HONO emissions observed above the snowpack [8,11]. We suggest that HONO is produced in the firn air either by gas phase reactions (e.g. $\text{NO} + \text{OH}$) or by heterogeneous reactions of NO_2 or HO_2NO_2 at the snow crystal surfaces. Several studies have demonstrated that the heterogeneous hydrolysis of NO_2 yields gas phase HONO (e.g. [61]). More recently, George et al. [62] demonstrated that HONO was produced with a high efficiency by the heterogeneous reaction of NO_2 with light absorbing organic compounds. Since Grannas et al. [35] reported contributions of phenols and further aromatic compounds to the organic content of snow samples collected at Summit, the suggested mechanism might contribute to the HONO formation in the firn air. However, whether the firn air concentrations of NO_x , OH, and HO_2NO_2 are high enough to produce significant amounts of HONO remains unresolved as discussed by Cotter et al. [21].

It has been proposed that the HONO flux out of or into the snowpack depends on the pH value of the snow [17,36]. Our model calculations indicate that the pH value of the QLL does not impact the formation rate of HONO in the snow: the formation is always negligible due to the small NO_2^- concentrations obtained in the model calculations. However, the pH can obviously determine if the HONO produced in the firn air is absorbed by the QLL or rather released to the atmosphere above the snowpack. While pH values can enhance the dissociation of HONO into H^+ and NO_2^- , thus increasing the solubility of HONO in the QLL, this effect should be most obvious at pH values around

the pK_s of HONO. Varying the pH around the pK_s by ± 1 means that either 90% or 10% of the HONO would be present in the not-dissociated form in the QLL. The measured snow pH represents an equilibrium value obtained from the melted snow sample. In other words, this is the pH of a solution containing all the electrolytes present in the snow sample. Recent laboratory experiments clearly demonstrated that the pH of the QLL can be significantly different compared to the melted ice [63]. At present it is not clear how the measured snow pH relates to the pH of the QLL. Further studies on natural snow samples are needed to investigate this value since it is the crucial parameter for the air–snow equilibrium of acidic and alkaline species.

Due to the small volume of the QLL, it still constitutes only a limited reservoir for HONO. However, as shown in Fig. 5, NO_2^- is unstable in the QLL, where it is destroyed with a rate of 9.5×10^{11} molecules $\text{L}_{\text{snow}}^{-1} \text{s}^{-1}$ for typical conditions at Summit. We can compare this destruction rate with observed deposition fluxes of HONO to snow surfaces. For example, a HONO flux of up to $120 \text{ nmol m}^{-2} \text{ h}^{-1}$ was observed in the Apennine mountains in Italy in spring [36]. This value corresponds to a HONO flux of 2.0×10^{13} molecules $\text{m}^{-2} \text{ s}^{-1}$. If we assume a typical snow density of 0.3 g cm^{-3} , the photochemical destruction in a snow layer with a depth of 7 cm is sufficient to destroy the deposited HONO completely. The conditions of the surface snow at Summit are probably significantly different compared to the springtime snow in the Apennines regarding the snow composition and temperature, the solar radiation intensities, and the pH of the snow. Nevertheless, the comparison indicates that the proposed photochemical mechanism for the surface snow is well able to explain the fate of the HONO deposited to the snow surface.

5. Summary and conclusions

We developed a comprehensive mechanism for the photochemical transformation of NO_3^- to NO_2^- in snow and further to more volatile nitrogen containing compounds like NO and NO_2 . Applying this mechanism to data obtained in different laboratory experiments, we adjusted unknown photolysis rates of NO_3^- and NO_2^- in artificial snow for the experimental conditions. The rates were further verified using previously published laboratory experiments and field studies. These comparisons demonstrate that (i) the general mechanism is able to capture the main features of the photochemical transformation of nitrogen compounds in snow and (ii) the adjusted rates can be applied to a wide range of conditions.

We adjusted the photochemical mechanism to typical summer conditions for the Greenland ice sheet. These simulations showed that the NO_2^- concentrations in the snow remained extremely low. NO_2^- remains still an important intermediate for the formation of NO_2 in the snow although the NO_2 formation is dominated by the photolysis of NO_3^- . A large fraction of the produced NO_2 is oxidized back to NO_3^- reducing the net NO_3^- destruction rate by 40%. The model calculations indicate that for summer conditions in Greenland, out of five NO_3^- molecules initially photolyzed in the snow, approximately three are released to the firm air in the form of NO_2 and two molecules

are re-oxidized back to NO_3^- . Comparisons of the modeled NO_2^- and NO_2 concentrations and the Henry's law constants of HONO and NO_2 further indicate that the HONO production within the snow is probably negligible. We suggest that HONO, which is readily emitted by the sun-lit snowpack, is formed in the firm air possibly by the heterogeneous reaction of NO_2 on the surface of the ice crystals.

The simulations with the photochemical mechanism further show that observed NO_x emissions are easily reconciled by the calculated NO_2 production in several centimeters of the surface snow. In addition, HONO deposition fluxes as observed onto more alkaline snow surfaces in lower latitudes are also in good agreement with the destruction rates for NO_2^- obtained with the model. In summary, we conclude that the proposed photochemical mechanism for the transformation of NO_3^- in snow represents a reasonable representation for the processes occurring in natural snow surfaces.

Nevertheless, further laboratory and field studies are needed to improve the mechanism and extend its applicability since several uncertainties remain. Although the mechanism is limited to nitrogen-containing compounds, the important role of other reactive species like the OH radical becomes already obvious. In agreement with previous experiments in the presence of radical scavengers [18,20], the model indicates that the reactions with OH radicals constitute important sinks for NO_2^- as well as for NO_2 (Fig. 5). Chu and Anastasio [64] concluded that the most important OH source in the snow is from the photolysis of H_2O_2 , which is omnipresent in natural snow. This shows that the recommended photochemical mechanism cannot account for all processes known to occur in the natural snowpack. Besides the sources of OH radicals, this concerns also the processing of organic compounds in the snow. Further studies are needed to develop a full photochemical reaction mechanism for the snow.

Additional uncertainties arise from the limited knowledge of the properties of the QLL. Furthermore, less reactive impurities like sea-salt components may increase the liquid fraction and, thus, reduce the QLL concentrations of the reactive compounds. Further laboratory and modeling studies are needed to characterize the QLL so that it can be represented better in the model.

Acknowledgement

Financial support by the Deutsche Forschungsgemeinschaft (DFG) is gratefully acknowledged.

References

- [1] F. Dominé, P.B. Shepson, Air–snow interactions and atmospheric chemistry, *Science* 297 (2002) 1506–1510.
- [2] R.E. Honrath, M.C. Peterson, S. Guo, J.E. Dibb, P.B. Shepson, B. Campbell, Evidence of NO_x production within or upon ice particles in the Greenland snowpack, *Geophys. Res. Lett.* 26 (1999) 695–698.
- [3] R.E. Honrath, M.C. Peterson, M.P. Dziobak, J.E. Dibb, M.A. Arsenaull, S.A. Green, Release of NO_x from sunlight-irradiated midlatitude snow, *Geophys. Res. Lett.* 27 (2000) 2237–2240.
- [4] B. Ridley, J. Walega, D. Montzka, F. Grahek, E. Atlas, F. Flocke, V. Stroud, J. Deary, A. Gallant, H. Boudries, J. Bottenheim, K. Anlauf, D. Worthy,

- A.L. Sumner, B. Splawn, P. Shepson, Is the Arctic surface layer a source and sink of NO_x in winter/spring? *J. Atmos. Chem.* 36 (2000) 1–22.
- [5] A.E. Jones, R. Weller, E.W. Wolff, H.-W. Jacobi, Speciation and rate of photochemical NO and NO_2 production in Antarctic snow, *Geophys. Res. Lett.* 27 (2000) 345–348.
- [6] A.E. Jones, R. Weller, P.S. Anderson, H.-W. Jacobi, E.W. Wolff, O. Schrems, H. Miller, Measurements of NO_x emissions from the Antarctic snowpack, *Geophys. Res. Lett.* 28 (2001) 1499–1502.
- [7] D. Davis, J.B. Nowak, G. Chen, M. Buhr, R. Arimoto, A. Hogan, F. Eisele, L. Mauldin, D. Tanner, R. Shetter, B. Lefer, P. McMurry, Unexpected high levels of NO observed at South Pole, *Geophys. Res. Lett.* 28 (2001) 3625–3628.
- [8] X. Zhou, H.J. Beine, R.E. Honrath, J.D. Fuentes, W. Simpson, P.B. Shepson, J.W. Bottenheim, Snowpack photochemical production of HONO: a major source of OH in the arctic boundary layer in springtime, *Geophys. Res. Lett.* 28 (2001) 4087–4090.
- [9] J.E. Dibb, M. Arsenault, M.C. Peterson, R.E. Honrath, Fast nitrogen oxide photochemistry in Summit, Greenland snow, *Atmos. Environ.* 36 (2002) 2501–2511.
- [10] R. Qiu, S.A. Green, R.E. Honrath, M.C. Peterson, Y. Lu, M. Dziobak, Measurements of $J_{\text{NO}_3^-}$ in snow by nitrate-based actinometry, *Atmos. Environ.* 36 (2002) 2563–2571.
- [11] R.E. Honrath, Y. Lu, M.C. Peterson, J.E. Dibb, M.A. Arsenault, N.J. Cullen, K. Steffen, Vertical fluxes of NO_x , HONO, and HNO_3 above the snowpack at Summit, Greenland, *Atmos. Environ.* 36 (2002) 2629–2640.
- [12] H.J. Beine, R.E. Honrath, F. Dominé, W.R. Simpson, J.D. Fuentes, NO_x during background and ozone depletion periods at Alert: fluxes above the snow surface, *J. Geophys. Res.* 107 (D21) (2002) 4584, doi:10.1029/2002JD002082.
- [13] H.J. Beine, F. Dominé, A. Ianniello, M. Nardino, I. Allegrini, K. Teinilä, R. Hillamo, Fluxes of nitrate between snow surfaces and the atmosphere in the European high Arctic, *Atmos. Chem. Phys.* 3 (2003) 335–346.
- [14] H.-W. Jacobi, R.C. Bales, R.E. Honrath, M.C. Peterson, J.E. Dibb, A.L. Swanson, M.R. Albert, Reactive trace gases measured in the interstitial air of surface snow at Summit, Greenland, *Atmos. Environ.* 38 (2004) 1687–1697.
- [15] D. Davis, G. Chen, M. Buhr, J. Crawford, D. Lenschow, B. Lefer, R. Shetter, F. Eisele, L. Mauldin, A. Hogan, South Pole NO_x chemistry: an assessment of factors controlling variability and absolute levels, *Atmos. Environ.* 38 (2004) 5375–5388.
- [16] J.E. Dibb, L.G. Huey, D.L. Slusher, D.J. Tanner, Soluble reactive nitrogen oxides at South Pole during ISCAT 2000, *Atmos. Environ.* 38 (2004) 5399–5409.
- [17] A. Amoroso, H.J. Beine, R. Sparapani, M. Nardino, I. Allegrini, Observation of coinciding arctic boundary layer ozone depletion and snow surface emissions of nitrous acid, *Atmos. Environ.* 40 (2006) 1949–1956.
- [18] R.E. Honrath, S. Guo, M.C. Peterson, M.P. Dziobak, J.E. Dibb, M.A. Arsenault, Photochemical production of gas phase NO_x from ice crystal NO_3^- , *J. Geophys. Res.* 105 (2000) 24183–24190.
- [19] Y. Dubowski, A.J. Colussi, M.R. Hoffmann, Nitrogen dioxide release in the 302 nm band photolysis of spray-frozen aqueous nitrate solutions. Atmospheric implications, *J. Phys. Chem. A* 105 (2001) 4928–4932.
- [20] Y. Dubowski, A.J. Colussi, C. Boxe, M.R. Hoffmann, Monotonic increase of nitrite yields in the photolysis of nitrate in ice and water between 238 and 294 K, *J. Phys. Chem. A* 106 (2002) 6967–6971.
- [21] E.S.N. Cotter, A.E. Jones, E.W. Wolff, S.J.-B. Baugitte, What controls photochemical NO and NO_2 production from Antarctic snow? Laboratory investigation assessing the wavelength and temperature dependence, *J. Geophys. Res.* 108 (D4) (2003) 4147, doi:10.1029/2002JD002602.
- [22] L. Chu, C. Anastasio, Quantum yields of hydroxyl radical and nitrogen dioxide from the photolysis of nitrate on ice, *J. Phys. Chem. A* 107 (2003) 9594–9602.
- [23] C.S. Boxe, A.J. Colussi, M.R. Hoffmann, D. Tan, J. Mastromarino, A.T. Case, S.T. Sandholm, D.D. Davis, Multiscale ice fluidity in NO_x photodesorption from frozen nitrate solutions, *J. Phys. Chem. A* 107 (2003) 11409–11413.
- [24] T. Blunier, G.L. Floch, H.-W. Jacobi, E. Quansah, Isotopic view on nitrate loss in Antarctic surface snow, *Geophys. Res. Lett.* 32 (2005) L13501.
- [25] C.S. Boxe, A.J. Colussi, M.R. Hoffmann, J.G. Murphy, P.J. Wooldridge, T.H. Bertram, R.C. Cohen, Photochemical production and release of gaseous NO_2 from nitrate-doped water ice, *J. Phys. Chem. A* 109 (2005) 8520–8525.
- [26] C.S. Boxe, A.J. Colussi, M.R. Hoffmann, I.M. Perez, J.G. Murphy, R.C. Cohen, Kinetics of NO and NO_2 evolution from illuminated frozen nitrate solutions, *J. Phys. Chem. A* 110 (2006) 3578–3583.
- [27] H.-W. Jacobi, T. Annor, E. Quansah, Investigation of the photochemical decomposition of nitrate, hydrogen peroxide, and formaldehyde in artificial snow, *J. Photochem. Photobiol. A* 179 (2006) 330–338.
- [28] G. Chen, D. Davis, J. Crawford, L.M. Hutterli, L.G. Huey, D. Slusher, L. Mauldin, F. Eisele, D. Tanner, J. Dibb, M. Buhr, J. McConnell, B. Lefer, R. Shetter, D. Blake, C.H. Song, K. Lombardi, J. Arnoldy, A reassessment of HO_x South Pole chemistry based on observations recorded during ISCAT 2000, *Atmos. Environ.* 38 (2004) 5451–5461.
- [29] J. Yang, R.E. Honrath, M.C. Peterson, J.E. Dibb, A.L. Sumner, P.B. Shepson, M. Frey, H.-W. Jacobi, A. Swanson, N. Blake, Impacts of snowpack emissions on deduced levels of OH and peroxy radicals at Summit, Greenland, *Atmos. Environ.* 36 (2002) 2523–2534.
- [30] M. Legrand, P. Mayewski, Glaciochemistry of polar ice cores: a review, *Rev. Geophys.* 35 (1997) 219–243.
- [31] R. Röthlisberger, M.A. Hutterli, E.W. Wolff, R. Mulvaney, H. Fischer, M. Bigler, K. Goto-Azuma, M.E. Hansson, U. Ruth, M.-L. Siggaard-Andersen, J.P. Steffensen, Nitrate in Greenland and Antarctic ice cores: a detailed description of post-depositional processes, *Ann. Glaciol.* 35 (2002) 209–216.
- [32] J.R. McCabe, C.S. Boxe, A.J. Colussi, M.R. Hoffmann, M.H. Thiemens, Oxygen isotopic fractionation in the photochemistry of nitrate in water and ice, *J. Geophys. Res.* 110 (2005) D15310, doi:10.1029/2004JD005484.
- [33] J. Mack, J.R. Bolton, Photochemistry of nitrite and nitrate in aqueous solution: a review, *J. Photochem. Photobiol. A* 128 (1999) 1–13.
- [34] A.L. Sumner, P.B. Shepson, Snowpack production of formaldehyde and its effect on the Arctic troposphere, *Nature* 398 (1999) 230–233.
- [35] A.M. Grannas, P.B. Shepson, T.R. Fillee, Photochemistry and nature of organic matter in Arctic and Antarctic snow, *Global Biogeochem. Cycles* 18 (GB1006) (2004), doi:10.1029/2003GB002133.
- [36] H.J. Beine, A. Amoroso, G. Esposito, R. Sparapani, A. Ianniello, T. Georgiadis, M. Nardino, P. Bonasoni, P. Cristofanelli, F. Dominé, Deposition of atmospheric nitrous acid on alkaline snow surfaces, *Geophys. Res. Lett.* 32 (2005) L10808, doi:10.1029/2005GL022589.
- [37] K.C. Clemitshaw, Coupling between the tropospheric photochemistry of nitrous acid (HONO) and nitric acid (HNO_3), *Environ. Chem.* 3 (2006) 31–34.
- [38] W. Liao, A.T. Case, J. Mastromarino, D. Tan, J.E. Dibb, Observations of HONO by laser-induced fluorescence at the South Pole during ANTCI 2003, *Geophys. Res. Lett.* 33 (2006) L09810, doi:10.1029/2005GL025470.
- [39] H.-W. Jacobi, B. Kwakye-Awuah, O. Schrems, Photochemical decomposition of hydrogen peroxide (H_2O_2) and formaldehyde (HCHO) in artificial snow, *Ann. Glaciol.* 39 (2004) 29–33.
- [40] D. Zehavi, J. Rabani, Pulse radiolytic investigation of O_{aq}^- radical ions, *J. Phys. Chem.* 75 (1971) 1738–1744.
- [41] G.C. Barker, P. Fowles, B. Stringer, Pulse radiolytic induced transient electrical conductance in liquid solutions. Part 2. Radiolysis of aqueous solutions of NO_3^- , NO_2^- and $\text{Fe}(\text{CN})_6^{3-}$, *Trans. Faraday Soc.* 66 (1970) 1509–1519.
- [42] H.H. Awad, D.M. Stanbury, Autoxidation of NO in aqueous solution, *Int. J. Chem. Kinet.* 25 (1993) 375–381.
- [43] J.L. Cheung, Y.Q. Li, J. Boniface, Q. Shi, P. Davidovits, D.R. Worsnop, J.T. Jayne, C.E. Kolb, Heterogeneous interactions of NO_2 with aqueous surfaces, *J. Phys. Chem. A* 104 (2000) 2655–2662.
- [44] T. Løgager, K. Sehested, Formation and decay of peroxyxynitrous acid: a pulse radiolysis study, *J. Phys. Chem.* 97 (1993) 6664–6669.
- [45] U.K. Klänning, K. Sehested, T. Wolff, Ozone formation in laser flash photolysis of oxoacids and oxoanions of chlorine and bromine, *J. Chem. Soc., Faraday Trans.* 80 (1984) 2969–2979.

- [46] H. Strehlow, I. Wagner, Flash photolysis in aqueous nitrite solutions, *Z. Phys. Chem. NF* 132 (1982) 151–160.
- [47] J.-Y. Park, Y.-N. Lee, Solubility and decomposition kinetics of nitrous acid in aqueous solution, *J. Phys. Chem.* 92 (1988) 6294–6302.
- [48] R. Sander, Compilation of Henry's Law Constants for Inorganic and Organic Species of Potential Importance in Environmental Chemistry, Version 3, 1999. <http://dionysos.mpch-mainz.mpg.de/~sander/res/henry.html>.
- [49] C. Girardet, C. Toubin, Molecular atmospheric pollutant adsorption on ice: a theoretical survey, *Surf. Sci. Rep.* 44 (2001) 159–238.
- [50] H. Bluhm, D.F. Ogletree, C.S. Fadley, Z. Hussain, M. Salmeron, The pre-melting of ice studied with photoelectron spectroscopy, *J. Phys. Condens. Matter* 14 (2002) L227–L233.
- [51] H. Cho, P.B. Shepson, L.A. Barrie, J.P. Cowin, R. Zaveri, NMR investigation of the quasi-brine layer in ice/brine mixtures, *J. Phys. Chem. B* 106 (2002) 11226–11232.
- [52] A. Döppenschmidt, H.-J. Butt, Measuring the thickness of the liquid-like layer on ice surfaces with atomic force microscopy, *Langmuir* 16 (2000) 6709–6714.
- [53] X. Wei, P.B. Miranda, C. Zhang, Y.R. Shen, Sum-frequency spectroscopic studies of ice interfaces, *Phys. Rev. B* 66 (2002) 085401.
- [54] J.E. Dibb, R.W. Talbot, J.W. Munger, D.J. Jacob, S.-M. Fao, Air-snow exchange of HNO_3 and NO_y at Summit, Greenland, *J. Geophys. Res.* 103 (1998) 3475–3486.
- [55] P. Hoffmann, V.K. Karandashev, T. Sinner, H.M. Ortner, Chemical analysis of rain and snow samples from Chernogolovka/Russia by IC, TXRF and ICP-MS, *Fresenius J. Anal. Chem.* 357 (1997) 1142–1148.
- [56] Y. Miura, H. Hamada, Ion chromatography of nitrite at the ppb level with photometric measurement of iodine formed by post-column reaction of nitrite with iodide, *J. Chromatogr. A* 850 (1999) 153–160.
- [57] A. Fernandez-Gutierrez, C. Cruces-Blanco, S. Cortacero-Ramirez, A. Segura-Carretero, Sensitive determination of inorganic anions at trace levels in samples of snow water from Sierra Nevada (Granada, Spain) by capillary ion electrophoresis using Calix[4]arene as selective modifier, *Chromatographia* 52 (2000) 413–417.
- [58] S.-M. Li, Particulate and snow nitrite in the spring arctic troposphere, *Atmos. Environ.* 27 (1993) 2959–2967.
- [59] M. Peterson, D. Barber, S. Green, Monte Carlo modeling and measurements of actinic flux levels in Summit, Greenland snowpack, *Atmos. Environ.* 36 (2002) 2545–2551.
- [60] E. Riordan, N. Minogue, D. Healy, P. O'Driscoll, J.R. Sodeau, Spectroscopic and optimization modeling study of nitrous acid in aqueous solution, *J. Phys. Chem. A* 109 (2005) 779–786.
- [61] B.J. Finlayson-Pitts, L.M. Wingen, A.L. Sumner, D. Syomin, K.A. Ramazan, The heterogeneous hydrolysis of NO_2 in laboratory systems and in outdoor and indoor atmospheres: an integrated mechanism, *Phys. Chem. Chem. Phys.* 5 (2003) 223–242.
- [62] C. George, R.S. Strekowski, J. Kleffmann, K. Stemmler, M. Ammann, Photoenhanced uptake of gaseous NO_2 on solid organic compounds: a photochemical source of HONO? *Faraday Disc.* 130 (2005) 195–210.
- [63] C. Robinson, C.S. Boxe, M.I. Guzmán, A.J. Colussi, M.R. Hoffmann, Acidity of frozen electrolyte solutions, *J. Phys. Chem. B* 110 (2006) 7613–7616.
- [64] L. Chu, C. Anastasio, Formation of hydroxyl radical from the photolysis of frozen hydrogen peroxide, *J. Phys. Chem. A* 109 (2005) 6264–6271.